Klotho controls the brain–immune system interface in the choroid plexus

Lei Zhu[a,1], Liana R. Stein[a,1], Daniel Kim[a], Kaitlyn Ho[a], Gui-Qiu Yu[a], Lihong Zhan[a], Tobias E. Larsson[b], and Lennart Mucke[a,c,2]

[a]Gladstone Institute of Neurological Disease, Gladstone Institutes, San Francisco, CA 94158; [b]Nephrology Unit, Department of Clinical Science, Intervention and Technology, Karolinska Institute, M 99 141 86 Stockholm, Sweden; and [c]Department of Neurology, University of California, San Francisco, CA 94158

Located within the brain's ventricles, the choroid plexus produces cerebrospinal fluid and forms an important barrier between the central nervous system and the blood. For unknown reasons, the choroid plexus produces high levels of the protein klotho. Here, we show that these levels naturally decline with aging. Depleting klotho selectively from the choroid plexus via targeted viral vector-induced knockout in *Klotho*^flox/flox mice increased the expression of multiple proinflammatory factors and triggered macrophage infiltration of this structure in young mice, simulating changes in unmanipulated old mice. Wild-type mice infected with the same Cre recombinase-expressing virus did not show such alterations. Experimental depletion of klotho from the choroid plexus enhanced microglial activation in the hippocampus after peripheral injection of mice with lipopolysaccharide. In primary cultures, klotho suppressed thioredoxin-interacting protein-dependent activation of the NLRP3 inflammasome in macrophages by enhancing fibroblast growth factor 23 signaling. We conclude that klotho functions as a gatekeeper at the interface between the brain and immune system in the choroid plexus. Klotho depletion in aging or disease may weaken this barrier and promote immune-mediated neuropathogenesis.

aging | choroid plexus | inflammation | klotho | macrophage

Aging is associated with a progressive increase in inflammatory alterations in the brain and other organs, a process that has been dubbed "inflammaging" (1). Biomarkers of inflammation are robust predictors of morbidity and mortality in older humans (1) and of age-related cognitive decline (2). The choroid plexus (CP) is an important gateway for the entry of immune cells into the central nervous system (CNS) (3, 4). Located within the ventricles of the brain, the CP consists of tight junction-bound epithelial cells resting upon a basal lamina and an inner stromal core. The stroma contains connective tissue and large capillaries with thin fenestrated endothelial walls and can harbor additional cell types, including dendritic cells with antigen-presenting capacity, macrophages, and granulocytes (3–5). The CP responds to signals from blood and cerebrospinal fluid (CSF) and supports the CNS by producing CSF, nutrients, and growth factors and by regulating pH, osmolality, ion concentrations, and immune molecule content in the extracellular space of the brain and spinal cord (3–8). Throughout life, the CP produces much higher levels of the antiaging protein α-klotho (klotho) (9) than other components of the CNS [ref. 10 and the Allen Brain Atlas (portal.brain-map.org)]. However, the functions klotho fulfills in the CP remain to be defined.

Klotho production in peripheral organs is highest in the kidney where it regulates vitamin D metabolism and the transport of phosphate and calcium (8, 11). Alternative splicing gives rise to two isoforms: secreted klotho (s-KL, amino acids 1 to 550 in mice) and full-length transmembrane klotho (m-KL, amino acids 1 to 1014 in mice) (11). The latter can be cleaved by sheddases of the ADAM family, resulting in proteolytic release of klotho (p-KL, amino acids 1 to ~960 in mice) into blood and CSF (11–13). *Klotho* hypomorphic (*kl/kl*) mice have a deletion in the 5' upstream region of the *klotho* gene, resulting in undetectable *klotho*

mRNA levels in organs that normally express the klotho gene, such as the brain and kidney (9). While the possibility that the *klotho* gene is slightly transcribed in these mutants remains, the effect of this deletion is markedly reduced klotho expression throughout the body and a premature aging phenotype that affects multiple peripheral organs, resulting in early death (9, 14). CNS alterations in *kl/kl* mice include hypomyelination, increased expression or phosphorylation of neurofilaments, synaptic loss, and behavioral impairments (14–16). Conceivably, at least some of these alterations result from the global reduction of klotho during early development and related systemic alterations. Whether more circumscribed reductions of klotho later in life also cause CNS pathology is not known. Here, we demonstrate that reducing klotho levels selectively in the CP disrupts the barrier between the immune system and the brain and promotes neuroinflammation.

Results

Aging Depletes Klotho in the CP. In brains of wild-type (WT) mice, klotho was expressed predominantly in the CP (Fig. 1*A* and *SI Appendix*, Fig. S1*A*) and to a lesser extent in the hippocampus (Fig. 1*A* and *SI Appendix*, Fig. S1*A*), consistent with previous reports (10, 17–19). Klotho levels in these structures were markedly reduced in *kl/kl* mice (Fig. 1 *B* and *C* and *SI Appendix*, Fig. S1*B*). In the CP, a 130-kDa doublet band, most likely representing m-KL and p-KL, was the predominant form of klotho detected by Western blot

---

Significance

Global depletion of klotho accelerates aging, whereas klotho overexpression counteracts aging-related impairments. Why klotho is expressed at much higher levels in the choroid plexus than in other brain regions is unknown. We demonstrate in mice that aging is associated with klotho depletion in the choroid plexus. Reducing klotho selectively within the choroid plexus triggered inflammation within this structure and enhanced activation of innate immune cells within an adjacent brain region following a peripheral immune challenge. In cell culture, we identified a signaling pathway by which klotho suppresses activation of macrophages. Our findings shed light on klotho functions in the choroid plexus and provide a plausible mechanism by which klotho depletion from this structure promotes brain inflammation during the aging process.
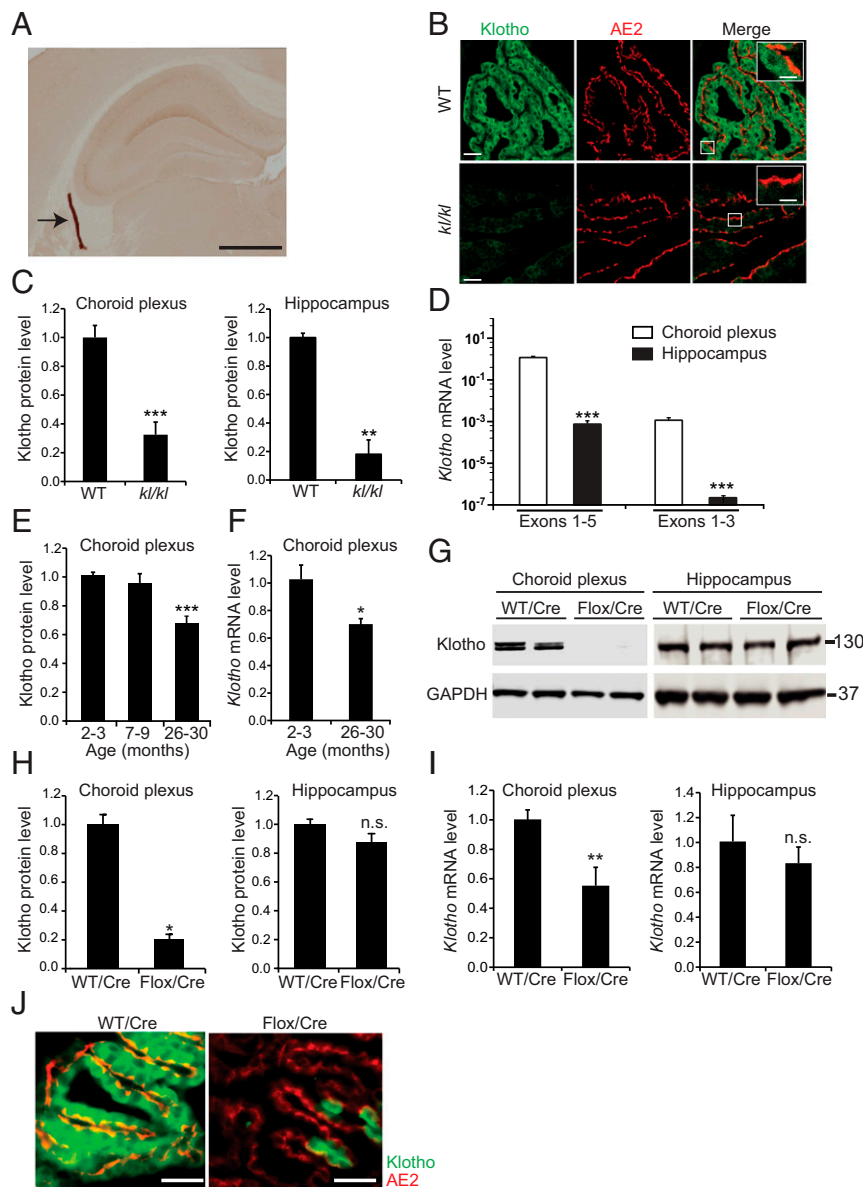

Fig. 1. Klotho depletion in the CP caused by aging or experimental manipulation. (*A*) CP (arrow) in the lateral ventricle of a 4-mo-old WT mouse visualized by klotho immunostaining of a coronal brain section. (*B*) Images of confocal optical sections of CPs in the lateral ventricles of 4-mo-old WT and *kl/kl* mice immunostained for klotho (green) and for the CP marker protein anion exchanger 2 (AE2). [Scale bars: 500 μm (*A*), 60 μm (*B*), 20 μm (*B*, *Inset*).] (*C*) Relative klotho levels in 2-mo-old mice (*C*, *E*, and *H*) were measured by Western blotting, normalized to GAPDH levels, and expressed relative to mean levels in WT controls. Relative *Klotho* mRNA levels (*F* and *I*) were calculated by the $2^{-\Delta\Delta C_T}$ method (75) using *Gapdh* mRNA as the internal reference and WT mice as the control. *n* = 11 to12 (CP) or 3 to 4 (hippocampus) mice per genotype. (*D*) Levels of *Klotho* mRNAs encoding the longer (exons 1 to 5) or shorter (exons 1 to 3) isoform in 4-mo-old WT mice determined by RT-qPCR. *n* = 8 (CP) or 15 (hippocampus) mice per group. Note that a log-10 scale was used because of the large differences in the levels of the *Klotho* transcripts. (*E* and *F*) CP levels of klotho protein (*E*) and *Klotho* mRNA (*F*) in WT mice. *n* = 13 mice per group. (*G* and *H*) Western blot (*G*) and klotho levels (*H*) in 7- to 8-mo-old WT and *Klotho*flox/flox (Flox) mice determined 5 to 6 mo after i.c.v. injection of AAV5-CMV-Cre (Cre). *n* = 4 mice per group. (*I*) *Klotho* mRNA levels in 20- to 24-mo-old WT and *Klotho*flox/flox (Flox) mice measured 11 mo after Cre injection (*n* = 4 to 8 mice per group). (*J*) Sagittal CP sections colabeled for klotho (green) and anion exchanger 2 (AE2) (red) from 20- to 24-mo-old WT and *Klotho*flox/flox mice obtained 11 mo after Cre injection. (Scale bars: 50 μm.) *P < 0.05, **P < 0.01, ***P < 0.001 vs. leftmost bar by unpaired, two-tailed *t* test (*C*, *F*, *H*, and *I*) or one-way ANOVA and Tukey test (*D* and *E*). n.s., not significant. Values in bar graphs are means ± SEM.

analysis (*SI Appendix*, Fig. S1 *B* and *C*) and will be referred to simply as klotho. In the CP and hippocampus of WT mice, s-KL (the short isoform) was undetectable at the protein level (*SI Appendix*, Fig. S1C); very low levels of *s-KL* mRNA were detected by quantitative RT-PCR using isoform-specific primers (Fig. 1D).

Klotho levels decrease with age in the plasma and CSF of humans (20), the white matter of monkeys (21), and the brain and kidney of mice (22, 23); however, the effects of aging on klotho expression in the CP appear to be unknown. In WT mice,

klotho levels in the CP were ∼34% lower at 26 mo of age than at 2 to 3 mo (Fig. 1E). This reduction was accompanied by an ∼32% decrease in *m-KL* mRNA levels (Fig. 1F), suggesting that aging affects *Klotho* expression in the CP at the pretranslational level. Although Massó et al. (23) found age-dependent reductions in hippocampal *m-KL* and *s-KL* mRNA levels in WT mice of a different genetic background, aging did not affect the hippocampal levels of klotho (*SI Appendix*, Fig. S1D) or *Klotho* mRNA (*SI Appendix*, Fig. S1E) in our WT mice.

Klotho Reduction in the CP Does Not Alter Hippocampal Klotho Levels.
To investigate the function of klotho in the CP, we reduced klotho levels specifically in this structure by intracerebroventricular (i.c.v.) injection of a viral vector encoding Cre recombinase into mice carrying two floxed *Klotho* alleles (*Klotho*[flox/flox]) (24). We used an adeno-associated virus serotype 5 (AAV5)-CMV construct that selectively targets expression to the CP upon i.c.v. injection (*SI Appendix*, Fig. S2A). Mice injected with AAV5-CMV-Cre-GFP (Cre) at 2 mo of age had ~70% less klotho in the CP at 7 to 8 mo of age (Fig. 1 *G* and *H*) when klotho levels had not yet decreased in WT controls (Fig. 1E). The klotho reduction in the CP of Cre-injected *Klotho*[flox/flox] mice was comparable with that in uninjected *kl/kl* mice (Fig. 1C and ref. 9). Selective reduction of klotho in the CP did not alter the gross morphology of this structure (*SI Appendix*, Fig. S2 *B–D*), the expression of the CP epithelial cell markers anion-exchanger 2 (Fig. 1J), aquaporin-1, cytokeratin, and CD31 (*SI Appendix*, Fig. S2 *C* and *D*), or the level and distribution of the tight junction protein claudin-1 (*SI Appendix*, Fig. S2D). AAV5-driven Cre expression was confined to the CP (*SI Appendix*, Fig. S2A) and reduced klotho levels similarly in the CPs of the lateral and fourth ventricles in *Klotho*[flox/flox] mice (*SI Appendix*, Fig. S3 *A* and *C*). No Cre expression or klotho reduction was detected in peripheral klotho-expressing tissues, such as the kidney (*SI Appendix*, Fig. S3 *B* and *D*).

Because m-KL is expressed abundantly in the CP and can be shed into the CSF as p-KL (12, 13, 17), it has been postulated that the CP functions as an important source of klotho for the brain parenchyma (17). However, klotho reduction in the CP did not alter klotho levels in the hippocampus (Fig. 1 *G–I*), suggesting that most, if not all, of the klotho in the hippocampus is generated locally and that CP-derived p-KL either does not reach the hippocampus or represents only a very small fraction of its overall klotho levels. The likeliest sources of klotho in the hippocampus are pyramidal neurons and dentate granule cells although they express much less klotho than CP epithelial cells (Fig. 1D, *SI Appendix*, Fig. S1B, and ref. 18).

Klotho Reduction Increases MHC II. Many aging-related alterations in the brain and other organs appear to involve inflammation (1). We therefore examined whether the reduced expression of klotho in the CP of old mice was associated with an increased expression of inflammatory mediators. One such mediator is the major histocompatibility complex class II (MHC II), whose expression by antigen-presenting cells in the brain increases with age (25, 26). In the CP, aging-related increases in MHC II are found primarily in antigen-presenting stromal cells, which have a highly irregular and elongated shape (27). Because of this shape, it can be difficult to differentiate between adjacent MHC II-positive cells. Therefore, we examined percent area occupied by MHC II immunoreactivity as a more reliable measure of MHC II expression in the CP. Consistent with the findings by Baruch et al. (27), MHC II immunoreactivity levels in the CP of uninjected WT mice were 5.6-fold higher at 22 to 23 mo than at 2 to 3 mo of age, and MHC II-positive cells were distinct from CP epithelial cells (Fig. 2 *A–C*).

To determine whether this increase in MHC II expression was a cause or consequence of the associated klotho reduction, we analyzed 19- to 22-mo-old WT and *Klotho*[flox/flox] mice 9 mo after i.c.v. injection of Cre. Selective reduction of klotho in the CP further increased MHC II expression in this structure by twofold (Fig. 2 *D* and *E*), suggesting that klotho reduction increases MHC II expression in the CP.

Klotho Regulates IFN-Related Genes. MHC II expression is regulated by interferons (28, 29), a complex family of proteins and peptides that induce the expression of cell-adhesion molecules and other immunologically relevant cell membrane constituents, control growth and differentiation, and activate natural killer cells and macrophages (30). The expression of inflammatory
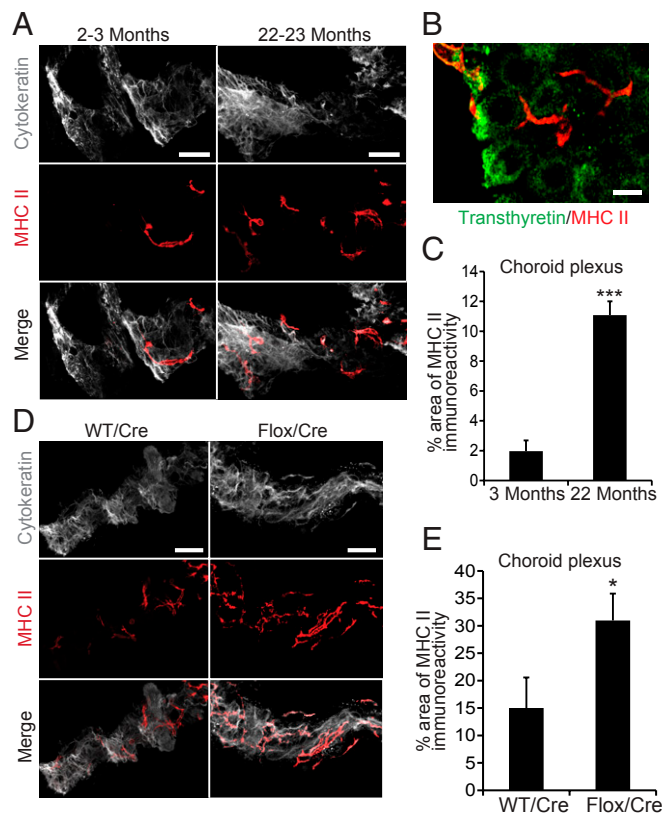

Fig. 2. Klotho depletion increases MHC class II expression in the CP. (*A–D*) MHC II immunoreactivity in the CP of uninjected young (2 to 3 mo) vs. old (22 to 23 mo) WT mice (*A–C*) and of Cre-injected 19- to 22-mo-old WT vs. *Klotho*[flox/flox] (Flox) mice measured 9 mo after i.c.v. injection (*D* and *E*). $n = 5$ to 7 mice per group. Coronal CP sections were double-labeled for MHC II (red) and for cytokeratin (gray) (*A* and *D*) or transthyretin (green) (*B*). [Scale bars: 100 μm (*A* and *D*), 30 μm (*B*).] *$P < 0.05$, ***$P < 0.001$ by unpaired, two-tailed *t* test. Values in bar graphs are means ± SEM.

regulators and mediators is altered in the CP of aged mice, and alterations in some of these factors can impair brain functions (3, 27, 31, 32). In the current study, we analyzed a selection of factors that (*i*) are expressed in the CP, (*ii*) are altered by aging, and (*iii*) represent diverse components of the innate immune system (27, 31, 32).

In WT mice, aging markedly increased the expression of intercellular adhesion molecule 1 (ICAM1) and IFN regulatory factor 7 (IRF7) in the CP (*SI Appendix*, Fig. S4A). Selective reduction of klotho in the CP of *Klotho*[flox/flox] mice also increased CP levels of ICAM1 and IRF7 (Fig. 3 *A–C*) and of mRNAs encoding ICAM1 (*Icam1*), IRF7 (*Irf7*), chemokine (C-C motif) ligand 17 (*Ccl17*), C-X-C motif chemokine 10 (*Cxcl10*), and CX3C chemokine receptor 1 (*Cx3cr1*) (*SI Appendix*, Fig. S4B). ICAM1 expression was localized to the surface membrane of CP epithelial cells, as demonstrated by double labeling of brain sections for ICAM1 and transthyretin (Fig. 3D) or aquaporin 1 (AQP1) (Fig. 3E). In contrast, klotho reduction did not change CP levels of mRNAs encoding IFN β (*Ifnβ*), TOLL-like receptor 9 (*Tlr9*), or IFN receptor 1 (*Ifnar1*) (*SI Appendix*, Fig. S4B).

Notably, *Klotho*[flox/flox] mice and WT controls were age- and strain-matched and injected with the same Cre-expressing viral construct. Furthermore, age-matched uninjected WT mice, Cre-injected WT mice, and uninjected *Klotho*[flox/flox] mice had similar klotho levels in the CP (*SI Appendix*, Fig. S3A). It is therefore unlikely that differences between Cre-injected WT and Cre-injected *Klotho*[flox/flox] mice resulted from mouse strain differences
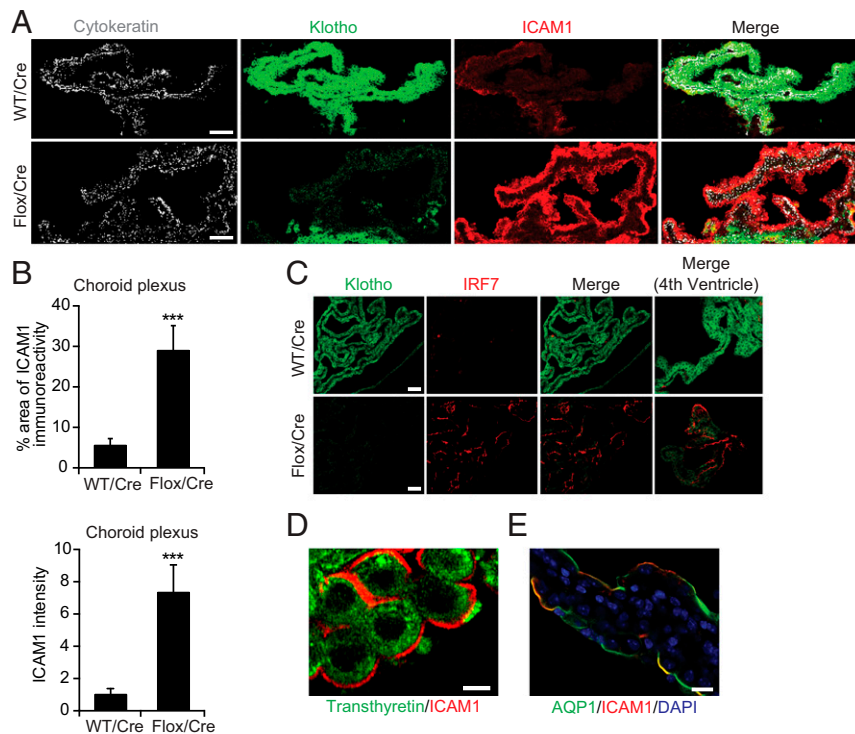
Fig. 3. Klotho reduction increases the expression of cytokine response factors in the CP. (A–C) ICAM1 (A and B) and IRF7 (C) immunoreactivity in the CP of 19- to 22-mo-old WT vs. *Klotho*^flox/flox (Flox) mice measured 9 mo after Cre injection. n = 5 to 7 mice per group. Sections of CP from the lateral ventricle (A–C) or fourth ventricle (C, *Rightmost* images) were colabeled for cytokeratin (gray), klotho (green), and ICAM1 (red) (A) or klotho (green) and IRF7 (red) (C). (Scale bars: 100 μm.) The percent of the cytokeratin-immunoreactive area that was also positive for ICAM1 was quantitated in B. (D and E) High magnification confocal images of the CP labeled for ICAM1 (red) and transthyretin (green) (D) or AQP1 (green) (E). [Scale bars: 25 μm (D), 50 μm (E).] ***P < 0.001 by unpaired, two-tailed t test. Values in bar graphs are means ± SEM.

or from effects of the viral infection. Nevertheless, in uninfected 2-mo-old *kl/kl* mice, we confirmed that global genetic reduction of klotho also increases the expression of IFN-related gene products in the CP (*SI Appendix*, Fig. S5 *A–C*). Neither of these klotho reduction strategies significantly altered the expression of such gene products in the hippocampus (*SI Appendix*, Fig. S5 *D and E*).

Klotho Reduction Causes Macrophage Infiltration. The CP is an important gateway for entry of immune cells into the CNS (3, 4, 33), and interferons can promote the transepithelial migration of leukocytes through the CP (34). In light of our discovery that klotho controls the expression of multiple immune mediators in the CP, we further tested our hypothesis that klotho is a key regulator of this gateway.

Cre-mediated klotho reduction increased the number of cells bearing the macrophage markers MAC-2 or IBA-1 (Fig. 4 *A–D*) in the CP of 19- to 22-mo-old *Klotho*^flox/flox mice. These cells were distinct from CP cells expressing transthyretin (Fig. 4*C*). To investigate the origin of this macrophage population, we immunostained the CP for lymphocyte antigen 6 complex (LY6C), which is primarily expressed on blood-derived monocytes (35). Klotho reduction in the CP increased the number of LY6C-positive cells in this structure (Fig. 4 *E and F*), presumably by increasing the production of immune modulators and chemoattractants by CP epithelial cells. The infiltration by putative peripheral macrophages was associated with increased expression of macrophage-related gene products with pro- or antiinflammatory activities, including mRNAs encoding arginase 1 (*Arg1*), nitric oxide synthase 2 (*Nos2*), and complement C1Q A chain (*C1qα*) (*SI Appendix*, Fig. S6 *A–C*). The CP of Cre-injected *Klotho*^flox/flox mice did not show significant changes in the numbers of T cells expressing CD3 or CD4 (*SI Appendix*, Fig. S6 *D*

and *E*). In contrast to Cre-injected *Klotho*^flox/flox mice, uninjected *kl/kl* mice showed no increases in the number of macrophages or the expression of macrophage-related gene products in the CP (*SI Appendix*, Fig. S7), although they had increased CP levels of at least some of the immune modulators (*SI Appendix*, Fig. S5) whose levels were increased in the CP of Cre-injected *Klotho*^flox/flox mice (*SI Appendix*, Fig. S4B and Table S1). Notably, *kl/kl* mice were analyzed at 2 mo of age because of their short life span, whereas Cre-injected *Klotho*^flox/flox mice were analyzed between 18 and 24 mo of age. Conceivably, the attraction of peripheral macrophages into the klotho-depleted CP takes time, requires aging-related cofactors that are missing in young *kl/kl* mice, or is counteracted by systemic alterations in these mice.

Klotho Reduction in the CP Promotes Microglial Activation. To determine whether klotho depletion from the CP affects other parts of the brain, we focused on the hippocampus, which is important for learning and memory and impaired by aging (36). Microglia, the primary immune cells of the hippocampus, are involved in neural plasticity, cognition, and neurological disease (37). Aging sensitizes these cells to activation by peripheral infections and lipopolysaccharide (LPS) injection, resulting in the excessive release of cytokines and chemokines that can impair cognitive functions (25, 38). To assess whether klotho reduction in the CP primes hippocampal microglia for activation, we challenged a cohort of 19- to 22-mo-old *Klotho*^flox/flox mice with two i.p. injections of low-dose ultrapure LPS (1 mg/kg) or saline 9 mo after they received an i.c.v. injection of AAV5-CMV-Cre (Cre) or AAV5-CMV-GFP (GFP). We then examined hippocampal levels of the microglial/macrophage marker IBA-1 and the microglia-specific marker TMEM119 by fluorescence microscopy. Microglial activation is associated with increased IBA-1
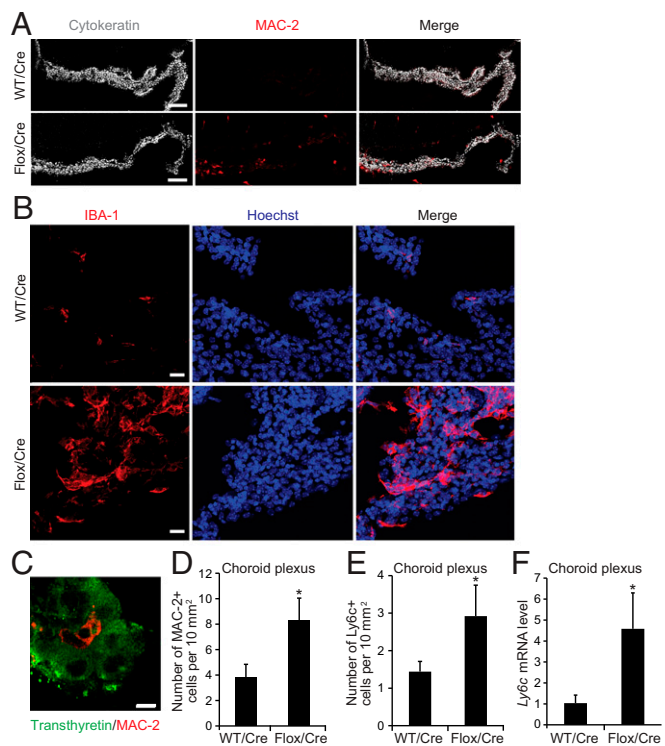
Fig. 4. Klotho reduction causes macrophage invasion into the CP. (A–E) Cells expressing the macrophage markers MAC-2 (A, C, and D), IBA-1 (B), or LY6C (E) and *Ly6c* mRNA levels (F) in the CP of 19- to 24-mo-old WT vs. *Klotho*^flox/flox (Flox) mice determined 9 mo after Cre injection. n = 4 to 9 mice per group. Sagittal CP sections were double-labeled for MAC-2 (red) and cytokeratin (gray) (A), IBA-1 (red) and Hoechst 33342 nuclear stain (blue) (B), or transthyretin (green) and MAC-2 (red) (C). [Scale bars: 100 μm (A), 50 μm (B), 25 μm (C).] *$P < 0.05$ by unpaired, two-tailed t test. Values in bar graphs are means ± SEM.

expression, retraction of processes, and enlargement of cell bodies (39). Both IBA-1 and TMEM119 immunostaining revealed morphological changes typical of microglial activation in the hippocampus of LPS-injected mice (Fig. 5A). Klotho reduction in the CP increased the number of IBA-1–positive cells (Fig. 5B) and the level of IBA-1 intensity (Fig. 5C) in the hippocampus after LPS injection. It also decreased the hippocampal TMEM119/IBA-1 area ratio in LPS-treated mice (Fig. 5D), suggesting retraction of microglial processes. These results indicate that klotho reduction in the CP exacerbates LPS-induced microglial activation, possibly through the release of inflammatory mediators from peripheral macrophages that have invaded the CP and from cells that normally reside in this structure, such as antigen-presenting cells.

Klotho Controls the NLRP3 Inflammasome. To unravel how klotho suppresses inflammation in the CP and other brain regions, we turned our attention to its role in controlling the production of vitamin D3 and of thioredoxin-interacting protein (TXNIP) (also known as vitamin D3 up-regulated protein 1). In peripheral tissues, klotho (m-KL > p-KL) functions as an obligate coreceptor for fibroblast growth factor 23 (FGF23) (40), which is present in blood and can be expected to traverse the fenestrated endothelial walls of CP capillaries. Thus, similar to klotho released from CP epithelial cells, blood-derived FGF23 should be able to interact with FGF receptors on macrophages that have infiltrated the stroma of the CP.

The FGF23/klotho signaling pathway suppresses the expression of 1-α-hydroxylase, which converts 25-hydroxycholecalciferol (25-VD$_3$) into 1,25-dihydroxycholecalciferol (1,25-VD$_3$ or cal-

citriol), the bioactive form of vitamin D, and increases the expression of 24-hydroxylase, which promotes the degradation of 1,25-VD$_3$ (11, 40, 41). 1,25-VD$_3$ can increase the expression of TXNIP, which promotes activation of the nucleotide binding oligomerization domain-like receptor protein 3 (NLRP3) inflammasome and increases oxidative stress by inhibiting thioredoxin activity (42–45). Since 1-α-hydroxylase is expressed in many cell types, including epithelial cells and activated macrophages (46), we hypothesized that klotho normally controls 1,25-VD$_3$ production in the CP and thereby suppresses TXNIP expression in cells that reside within or can infiltrate this structure.

Compared with controls, Cre-injected *Klotho*^flox/flox mice and uninjected *kl/kl* mice had increased CP levels of *Cyp27b1* mRNA (Fig. 6 A and B), which encodes 1-α-hydroxylase. Both groups of mice also had increased levels of *Txnip* mRNA and TXNIP protein in the CP (Fig. 6 C–G), suggesting that klotho in the CP may control the production of inflammatory mediators and the entry of immune cells by suppressing local 1,25-VD$_3$ production and downstream inflammasome activation by TXNIP.

In contrast, *Txnip* mRNA levels in the hippocampus of Cre-injected *Klotho*^flox/flox mice and uninjected *kl/kl* mice were not significantly different from those of their respective control littermates (*SI Appendix*, Fig. S8 A and B). *Txnip* mRNA levels in the kidney were also normal in *kl/kl* mice, despite profound reductions of klotho in this organ (*SI Appendix*, Fig. S8 C and D). These findings suggest that klotho has an important role in controlling *Txnip* expression in some cell types, but not others. In *kl/kl* mice, in which klotho levels are reduced during early development, this function of klotho may also be obscured by compensatory mechanisms.

Although macrophages do not appear to express full-length transmembrane klotho (47), their biological activity could be
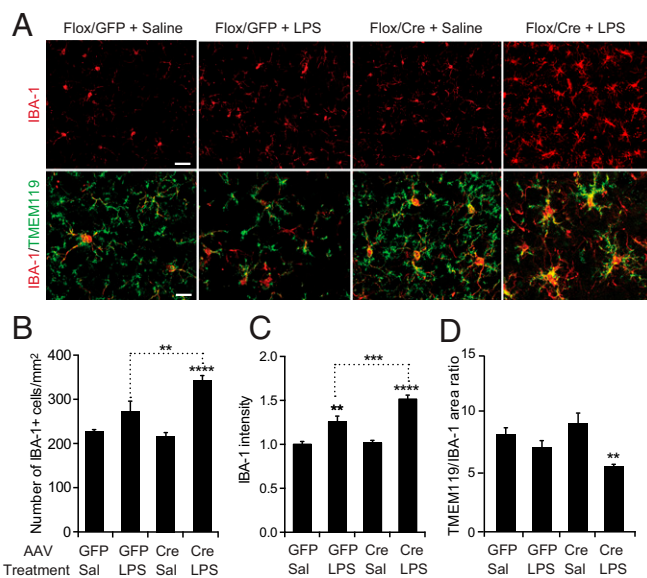

Fig. 5. Klotho reduction in CP primes hippocampal microglia for activation. (A) Hippocampal sections colabeled for IBA-1 (red) and TMEM119 (green) from 19- to 22-mo-old *Klotho*^flox/flox (Flox) mice obtained 9 mo after i.c.v. injection of AAV5-CMV-Cre (Cre) or AAV5-CMV-GFP (GFP) and imaged by fluorescence microscopy. Mice received i.p. injections of saline (Sal) or ultrapure LPS (1 mg/kg) 28 h and 4 h before sacrifice. [Scale bars: 50 μm (Upper), 25 μm (Lower).] (B–D) Relative hippocampal levels of IBA-1–positive cells (B), IBA-1 fluorescence intensity (C), and TMEM119 to IBA-1 area ratio (D) in mice exposed to these treatments (n = 4 to 8 mice per group). Mean levels in GFP/Sal-treated mice were defined as 1.0. **$P < 0.01$, ***$P < 0.001$, and ****$P < 0.0001$ by two-way ANOVA and Holm-Sidak's test. Values are means ± SEM.
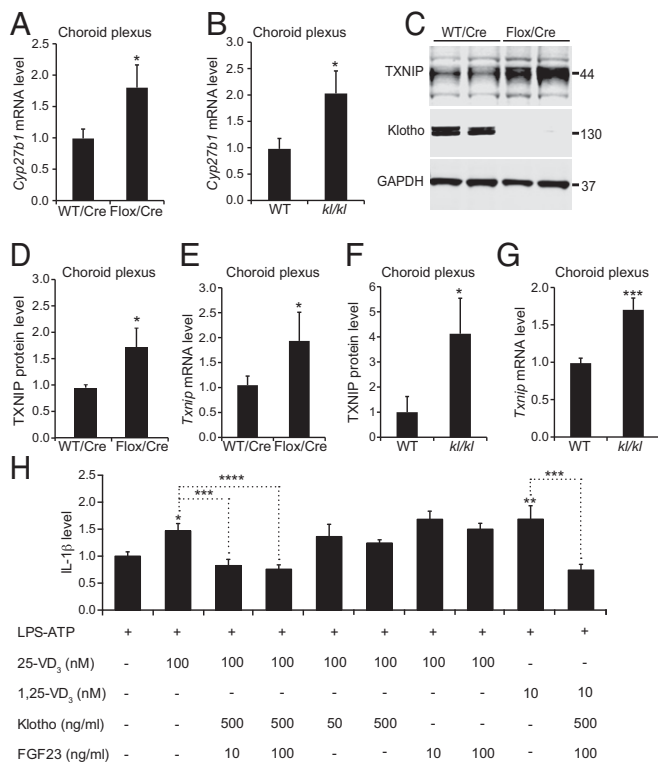
Fig. 6. Klotho controls regulators of the NLRP3 inflammasome. (*A* and *B*) CP levels of *Cyp27b1* mRNA in 20- to 24-mo-old WT vs. *Klotho*flox/flox (Flox) mice (*n* = 8 to 9 per group) measured 9 mo after Cre injection (*A*) and in uninjected 2-mo-old WT vs. *kl/kl* mice (*n* = 12 per group) (*B*). (*C*–*G*) Levels of TXNIP (*C*, *D*, and *F*) and klotho (*C*) protein and of *Txnip* mRNA (*E* and *G*) in 7- to 8-mo-old (*C* and *D*) or 20- to 24-mo-old (*E*) WT vs. *Klotho*flox/flox (Flox) mice (*n* = 4 per group) measured 5 (*C* and *D*) or 11 (*E*) mo after Cre injection and in uninjected 2-mo-old WT vs. *kl/kl* mice (*n* = 12 per group) (*F* and *G*). Relative protein and mRNA levels were determined as described in Fig. 1*H*. (*H*) Relative IL-1β levels in culture medium of bone marrow-derived primary macrophages from WT mice determined by ELISA on days in vitro 7 to 10 after treatment with LPS (100 EU/mL for 20 h; start time: 0 h) and ATP (1 mM for 1 h; start time: 20 h). Cultures were pretreated by adding vehicle or one or more of the following: 25-VD₃ (time: −1 h), 1,25-VD₃ (time: −1 h), klotho (time: −2 h), FGF23 (time: −2 h). *n* = 4 independent experiments, each of which included three to four wells per condition. IL-1β levels measured after pretreatment with vehicle and LPS/ATP stimulation were defined as 1.0. *P < 0.05, **P < 0.01, ***P < 0.001, ****P < 0.0001 vs. leftmost bar or as indicated by brackets (one-way ANOVA and Bonferroni test). Values in bar graphs are means ± SEM.

altered by klotho released from other cells (40). To further dissect the mechanisms by which klotho released from CP epithelial cells might control NLRP3 activation in macrophages, we exposed cultures of primary bone marrow-derived macrophages to recombinant klotho (p-KL) and other immune modulators. NLRP3 is a sensitive innate immune sensor that is activated by diverse stress signals (48). Its activation increases caspase 1 activity, resulting in the release of potent immune mediators, such as interleukin-1β (IL-1β), that may link inflammation to cognitive decline in aging (49). To activate NLRP3, we treated macrophage cultures with LPS and ATP (50). As expected, this treatment markedly increased IL-1β levels in the medium of macrophages from WT mice, but not of macrophages from *Nlrp3*⁻/⁻ or *Casp1/4*⁻/⁻ mice (*SI Appendix*, Fig. S9), which lack NLRP3 (51) or caspases 1 and 4 (52, 53), respectively. Pretreatment of macrophages with 1,25-VD₃, or with its immediate precursor, 25-VD₃, enhanced the LPS/ATP-induced macrophage activation (Fig. 6*H*), consistent with previous findings (54).

Pretreatment of macrophages with a combination of klotho and FGF23 blocked the vitamin D₃-induced enhancement of IL-1β release (Fig. 6*H*) whereas klotho or FGF23 alone had no significant modulatory effects (Fig. 6*H*). Interestingly, FGF23/klotho blocked the enhancement of LPS/ATP-induced IL-1β release by both 25-VD₃ and 1,25-VD₃ (Fig. 6*H*). This result suggests that FGF23/klotho signaling suppresses NLRP3 activation, not only by reducing the expression of 1-α-hydroxylase (Fig. 6 *A* and *B*), which generates 1,25-VD₃ from 25-VD₃, but also by counteracting 1,25-VD₃ downstream, possibly by promoting its degradation or blocking its effect on *Txnip* expression. Thus, FGF23/klotho signaling suppresses 1,25-VD₃–dependent inflammasome activation in macrophages, and depletion of klotho from the CP may increase the release of proinflammatory cytokines by infiltrating macrophages, which—in turn—could attract additional macrophages from the periphery and prime microglia in the brain parenchyma for activation (Fig. 5).

Discussion

Our findings suggest that klotho in the CP functions as a gatekeeper between the immune system and the CNS. The high level of klotho expressed in the CP of juvenile and adult mice, humans, and other mammals probably limits the penetration of this barrier by peripheral immune cells and suppresses the production of inflammatory mediators that could harm the CNS. We found that *Klotho* expression in the CP decreases with age and that experimental reduction of klotho levels specifically in this structure promotes the entry of peripheral macrophages and markedly increases the production of multiple proinflammatory mediators. Because similar proinflammatory changes occur during the natural aging process, the age-related decline in *Klotho* expression may contribute to the aging-related inflammation of the CNS. Because the CP produces and is bathed in CSF, inflammatory mediators produced in the CP are likely to reach other parts of the CNS via the CSF circulation (55), including the parenchyma of the brain and spinal cord, where they might contribute—by themselves or in combination with other factors—to the aging-related decline in neural functions (56). Indeed, experimental reduction of klotho in the CP exacerbated microglial activation in the hippocampus following peripheral injections of relatively low doses of LPS in the current study, suggesting that klotho depletion from the CP could contribute to the age-dependent "priming" of microglia for activation by peripheral infections (25, 38). Microglial activation and elevated IL-1β have been associated with deficits in synaptic plasticity in the hippocampus (57).

A more detailed comparison of the results we obtained after experimentally reducing klotho levels in the CP of mice to those reported to spontaneously develop in the CP of aged mice reveals both similarities and differences. For example, klotho reduction in the CP increased the expression of IRF7, a key regulator of type I IFN (IFNα/β) responses, which have important roles in adaptive and innate immunity (58). IRF7 is also increased in the CP of aged mice and humans (32). In a similar vein, arginase-1 expression in the CP was increased in mice with selective klotho reduction in the CP (this study) as well as in aged mice (27). In contrast, we found increased levels of *Icam1*, *Cxcl10*, and *Ccl17* mRNAs and of ICAM1 protein in the CP of mice with reduced klotho expression, whereas others found decreased levels of these gene products in the CP of aged mice (32). Some of these differences may reflect the fact that processes other than klotho reduction also affect the CP during aging and may override changes caused by klotho depletion. Other differences may have methodological or other reasons. For example, Baruch et al. reported increased IRF7 but decreased ICAM1 levels in the CP of aged mice (32), whereas CP levels of both proteins were increased in our aged mice, consistent with the results we obtained after reducing klotho levels in the CP of *Klotho*flox/flox mice by Cre injection.

NEUROSCIENCE

Our study provides insights into the mechanisms by which klotho may control the immune system/CNS interface in the CP. In combination, our in vivo and in vitro data support the hypothesis that klotho produced by CP epithelial cells suppresses the activation of the NLRP3 inflammasome in macrophages and possibly other cells, including the CP epithelial cells themselves, through FGF23/klotho signaling, counteracting 1,25-VD$_3$, and inhibiting 1,25-VD$_3$–dependent $Txnip$ expression. TXNIP, which was increased in the CP after klotho reduction, can directly increase the expression of proinflammatory gene products that promote leukocyte infiltration into the CNS, including ICAM-1 (59). TXNIP also promotes activation of the NLRP3 inflammasome, a process that probably contributes causally to multiple aging-related deficits and aging-related diseases, including cognitive decline and neurodegenerative disorders (49, 60).

Although TXNIP-dependent activation of the NLRP3 inflammasome is a plausible mechanism for many of the effects of klotho reduction we observed, our study was not designed to exclude alternative mechanisms by which klotho reduction in the CP might contribute to aging-related alterations of the CNS (5). Both klotho and the CP probably have diverse functions (3, 4, 6, 11, 33, 61). For example, klotho also attenuates the NF-κB pathway (62), which could contribute to the increase in ICAM1 expression after klotho reduction. Similarly, increased expression of TXNIP could affect multiple processes besides inflammation (42, 45). Another limitation of our study is that we did not systematically compare the effects of klotho reduction in CPs of all ventricles, which share many but not all properties (6).

In contrast to the genetic reduction of klotho in kl/kl mice, the injection of a Cre-expressing viral vector into $Klotho^{flox/flox}$ mice allowed us to (*i*) restrict klotho reduction specifically to the CP, (*ii*) avoid potential confounding effects of klotho reduction during early development, and (*iii*) lower klotho levels at distinct time points. Surprisingly, the viral vector approach revealed that klotho production by the CP is not needed to maintain normal klotho levels in the brain parenchyma, at least not in the hippocampus, where neurons produce low levels of klotho (18).

Despite the distinct ways in which klotho levels were reduced in the two models, we confirmed in uninjected kl/kl mice several of the findings we obtained in Cre-injected $Klotho^{flox/flox}$ mice, highlighting the robustness of these findings. Alterations of the CP observed in both models included increased levels of $Cyp27b1$ mRNA, $Txnip$ mRNA, and mRNAs encoding IFN-related factors, such as ICAM1, CCL17, and CXCR1. However, some changes we observed in Cre-injected $Klotho^{flox/flox}$ mice between 18 and 24 mo of age were not seen in uninjected kl/kl mice at 2 mo of age, including increased numbers of MAC-2- and Ly6C- positive cells and increased expression of the macrophage markers $Nos2$ and $Arg1$ in the CP. It is conceivable that these changes emerge over time, require aging-related cofactors that are missing in young kl/kl mice, or are prevented in kl/kl mice by the activation of compensatory processes during early development.

Increased numbers of monocytes, macrophages, and T cells have been identified in the kidneys of heterozygous $Klotho$ hypomorph ($kl/+$) mice (63). Our kl/kl mice had elevated TXNIP levels in the CP but not in the kidney. The latter discrepancy may reflect differences in cell type-specific inflammatory mechanisms, as reported for NLRP3 and receptors on macrophages and epithelial cells (64).

Reduced klotho levels and increased IL-1β levels have also been observed in the CP of rats exposed to chronic unpredictable stress, an experimental paradigm that causes behavioral alterations in rodents reminiscent of endogenous depression in humans (19). IL-1β also elicits depression-related behaviors in rodents (65). Our findings may also be relevant to Alzheimer's disease, in which klotho levels are decreased in the CSF (20, 23) and brain inflammation may have a critical pathogenic role (66–68).

Interestingly, global vitamin D$_3$ deficiency is a risk factor for age-related cognitive decline (69). Since vitamin D$_3$ has diverse effects throughout the body (69), it is tempting to speculate that high levels of klotho in the CP curtail immune invasion of the CNS via this important gateway by locally counteracting vitamin D$_3$ through FGF23/klotho signaling and reducing IFN/NLRP3-related gene expression, enabling the organism to benefit from useful vitamin D$_3$ effects elsewhere. Further investigation of klotho's immune-regulatory roles in the CP may identify therapeutic strategies to block entry of harmful cells and factors into the CNS through the blood–CSF barrier, which might help counteract cognitive decline in elderly people and inflammaging-related neurological disorders.

Methods

Mice and Treatments. $Klotho^{flox/+}$ mice (24) were interbred to generate $Klotho^{flox/flox}$ and $Klotho^{+/+}$ littermates on the same C57BL/6J background. CP-specific ablation of $Klotho$ in $Klotho^{flox/flox}$ mice was achieved by stereotaxically injecting 2 μL of high-titer (1 to 10 × 10^{12}/mL) AAV5-CMV-Cre-GFP (AAV5.CMV.HI.Cre.WPRE.SV40; Virovek) into the left lateral ventricle [coordinates: −1 mm mediolateral (M/L), −0.22 mm anteroposterior (A/P), and −2.5 mm dorsoventral (D/V) from the bregma]. Stereotaxic injections were carried out as described (70). WT mice injected with AAV5-CMV-Cre-GFP and in some cases $Klotho^{flox/flox}$ mice injected with AAV5-CMV-GFP (AAV5.CMV.HI.eGFP.WPRE.SV40; Virovek) served as negative controls. Overexpression of klotho in the hippocampus was achieved by injection of lentivirus encoding full-length klotho (Lenti-FUW2-klotho) into the dentate gyrus and CA1. The kl/kl mouse line (9) was obtained from M. Kuro-o (National Institute of Neuroscience, Kodaira, Tokyo) and the $Nlrp3^{−/−}$ line (51) from A. Ma (University of California, San Francisco, CA) $Casp1/4^{−/−}$ mice (52) were obtained from The Jackson Laboratory (strain 16621). Some mice received two separate i.p. injections of LPS (1 mg/kg; LPS-055: EB5; InvivoGen) 20 h apart and were perfused as described below 4 h after the second injection. Experimental and control groups were age-matched and littermates. Mice were maintained on a 12-h light/dark cycle, and experiments were conducted during the light cycle. Mice had free access to food (PicoLab Rodent Diet 20, 5053; LabDiet) and water, were housed 2 to 5 per cage. All procedures were approved by the Institutional Animal Care and Use Committee of the University of California, San Francisco.

Isolation of Mouse Tissues. Mice were anesthetized with Avertin (0.025 mg/mL) and perfused transcardially with 0.9% saline. Hemibrains were removed and drop-fixed in 4% paraformaldehyde overnight at 4 °C or flash-frozen in liquid nitrogen and stored at −80 °C. Frozen hemibrains were thawed in cold 1× PBS containing Halt Protease and Phosphatase Inhibitor Mixture (78447; Thermo Fisher Scientific) and microdissected immediately. The intact choroid plexus (CP) was removed first to avoid contaminating other tissues. Microdissected tissues were immediately frozen on dry ice and kept at −80 °C.

Primary Macrophage Cultures. Primary macrophages were prepared from 3- to 5-mo-old WT C57BL/6J mice as described (71). Femur bone marrow was extracted and mechanically dissociated in RPMI-1640 medium (Life Technologies). The cells were cultured in RPMI-1640, 10% FBS, 20 mM penicillin/streptomycin and 20 ng/mL macrophage colony-stimulating factor (ProSpec) at 2 × 10^6 cells per non-TC grade sterile 100-mm Petri dish (Corning). After 3 d, cells were dissociated in ice-cold PBS and replated in 12-well plates at 1 × 10^5 per well. Experiments were done on confluent cultures (typically days in vitro 7 to 8). Cultures were treated with ultrapure LPS (10^4 units/mL) for 16 to 24 h and harvested for analysis. Some cultures were incubated for an additional 4 h with ATP (1 mM; Sigma). In some cases, recombinant klotho (R&D Systems) and FGF-23 (R&D Systems) were added 1 h before LPS. After treatment, cells were washed once with PBS and collected for protein or mRNA analysis.

Immunohistochemistry. Brain sections were prepared and immunostained as described (72–74). Briefly, hemibrains were drop-fixed in 4% paraformaldehyde overnight, washed in cold PBS, equilibrated in 30% sucrose for ≥48 h, and stored at 4 °C. Hemibrains were sectioned (30 μm) on a freezing microtome, immunostained, and imaged with a digital microscope (BZ-9000; Keyence) or a laser-scanning microscope (LSM 880; Zeiss). Except for MHC II, antigen retrieval was performed using 10 mM citrate buffer at 105 °C for 20 min. After cooling at room temperature for at least 45 min, sections were incubated with 3% H$_2$O$_2$ for 15 min to quench endogenous peroxidase, washed four times in PBS, incubated in blocking/permeabilization solution containing 10% normal goat

serum and 0.3% Triton-X in PBS for ≥45 min, and incubated for ≥24 h with primary antibodies in 5% normal goat serum and 0.1% Triton X-100 in PBS at room temperature (dilutions provided in *SI Appendix*, Table S2). After three washes in PBS, sections were incubated with secondary antibodies (1:500; Invitrogen) and Hoechst 33342 (H33570; Thermo Scientific) diluted in 2% normal goat serum and 0.1% Triton X-100 in PBS for 2 h at room temperature. CLAUDIN-1 was detected with TSA-Plus cyanine 5 kits (PerkinElmer). Negative controls included omission of primary or secondary antibodies. High-resolution imaging was done with a Zeiss LSM 880 or a Keyence BZ-9000 automated microscope system. The Zeiss LSM 880 inverted scanning confocal microscope (Carl Zeiss Microscopy) was equipped with two photomultiplier tube (PMT) detectors, a high-sensitivity Gallium arsenide phosphide (GaAsP) detector, and a 32-GaAsP Airyscan superresolution detector and run by Zeiss Zen imaging software. The Keyence BZ-9000 inverted epifluorescence microscope was equipped with a 12-bit monochrome camera with red, green, and blue (RGB) capability. Unless indicated otherwise, all CP images were from CP in the lateral ventricles. For confocal microscopy, images were taken in z-stacks (2- to 4-μm steps) through immunoreactive areas. Z-stacks were analyzed with ImageJ or with Imaris software (Bitplane). For each section, numbers of cells positive for IRF7, ICAM1, MAC-2, or LY6C in the CP were normalized to the CP area in any given section; two to five sections were analyzed per mouse, and positive cells per area were averaged to generate a single value for each mouse (*n*). For quantitation of IBA-1 immunoreactivities, sections were stained as described above and imaged on a Versa Slide Scanner (Leica Systems) in z-stacks of 2-μm steps. The images were then batch-processed and analyzed using a macro developed in-house and the following functions. Areas of TMEM119 and IBA-1 immunoreactivity were measured by applying an adaptive threshold function (https://sites.google.com/site/qingzongtseng/adaptivethreshold). IBA-1–positive cells were counted automatically in the same images using the analyzed particle function of ImageJ.

Western Blotting. CPs from the fourth and lateral ventricles were combined for each mouse (except for *SI Appendix*, Fig. S3 in which they were analyzed separately), homogenized in radioimmunoprecipitation assay (RIPA) buffer containing Halt Protease and Phosphatase Inhibitor Mixture (Thermo Scientific), and sonicated (Episonic 1000; Epigentek) at amplitude 40 for 5 min; protein concentrations were determined by the bicinchoninic acid (BCA) method. Equal amounts of total protein (10 to 20 μg for CP and 20 to 30 μg for hippocampus and kidney) were loaded in 1× NuPAGE LDS sample buffer (NP0007; Thermo Fisher Scientific) and 1× Sample Reducing Agent (NP0009; Thermo Fisher Scientific), separated on NuPAGE 4 to 12% Bis-Tris gels (WT1403A; Thermo Fisher Scientific) at 200 V for 1.0 to 1.5 h in ice-cold 1× NuPAGE MOPS SDS running buffer (NP0001-02; Thermo Fisher Scientific). Gels were wet-transferred to nitrocellulose membranes (16 h, 25 V). The

blots were then blocked with Odyssey Blocking Buffer (927-40000; LI-COR) for 1 h at room temperature, incubated with primary antibodies (*SI Appendix*, Table S2) overnight at 4 °C, washed with PBS containing 0.05% Tween 20 (PBST) three to four times for 5 min at room temperature, incubated with secondary antibodies conjugated to IRDye (0.1 μg/mL; Li-COR) for 1 h at room temperature, and washed in PBST three to four times for 5 min at room temperature. Protein bands were visualized with an Odyssey CLx Infrared Imaging System (LI-COR) and quantified with Image Studio Software (LI-COR) following the manufacturer's instructions. The mean target protein:GAPDH ratio in WT mice was defined as 1.0.

Quantitative Real-Time RT-PCR. Total RNA from mouse CPs from lateral and fourth ventricles or hippocampus was isolated with RNeasy Kits (74106; Qiagen) and reverse-transcribed with High-Capacity cDNA Reverse Transcription Kits (Thermo Fisher Scientific). After reverse transcription, quantitative real-time PCR was conducted with an ABI Prism 7900HT Sequence Detection System and SYBR Green Nucleic Acid Detection Kit or TaqMan Gene Expression Master Mix (Thermo Fisher Scientific) and TaqMan primers (Applied Biosystems) (*SI Appendix*, Table S3). Levels of each target mRNA were detected with FAM dye. Normalized relative target mRNA levels were calculated by the $2^{-\Delta\Delta C_T}$ method (75) using GAPDH mRNA levels (detected with VIC dye in the same well) as the internal reference and expressed relative to mean values in the control group. Primer sequences used to detect transcripts encoding distinct klotho isoforms with the SYBR Green PCR method are shown in *SI Appendix*, Table S4.

Statistical Analysis. Prism (version 5; GraphPad), R (R Development Core Team, www.R-project.org/), and Microsoft Excel were used for statistical analyses. "*n*" refers to the number of mice for all figures except Fig. 6, in which "*n*" refers to independent experiments. Differences between genotypes and treatments were assessed by unpaired, two-tailed *t* test with Welch's correction or by one-way or two-way ANOVA and Bonferroni, Holm-Sidak, or Tukey post hoc tests. $P < 0.05$ was considered significant. Results were collected blinded to genotype and treatment of mice and cell cultures. Biological units were randomized during assays, sampling, and analysis.

1. Franceschi C, Garagnani P, Vitale G, Capri M, Salvioli S (2017) Inflammaging and 'Garb-aging'. *Trends Endocrinol Metab* 28:199–212.
2. DeCarlo CA, Tuokko HA, Williams D, Dixon RA, MacDonald SW (2014) BioAge: Toward a multi-determined, mechanistic account of cognitive aging. *Ageing Res Rev* 18:95–105.
3. Deczkowska A, Baruch K, Schwartz M (2016) Type I/II interferon balance in the regulation of brain physiology and pathology. *Trends Immunol* 37:181–192.
4. Kaur C, Rathnasamy G, Ling EA (2016) The choroid plexus in healthy and diseased brain. *J Neuropathol Exp Neurol* 75:198–213.
5. Emerich DF, Skinner SJ, Borlongan CV, Vasconcellos AV, Thanos CG (2005) The choroid plexus in the rise, fall and repair of the brain. *BioEssays* 27:262–274.
6. Lun MP, et al. (2015) Spatially heterogeneous choroid plexus transcriptomes encode positional identity and contribute to regional CSF production. *J Neurosci* 35:4903–4916, and erratum (2015) 35:8686.
7. Brinker T, Stopa E, Morrison J, Klinge P (2014) A new look at cerebrospinal fluid circulation. *Fluids Barriers CNS* 11:10.
8. Lindberg K, et al. (2014) The kidney is the principal organ mediating klotho effects. *J Am Soc Nephrol* 25:2169–2175.
9. Kuro-o M, et al. (1997) Mutation of the mouse klotho gene leads to a syndrome resembling ageing. *Nature* 390:45–51.
10. German DC, Khobahy I, Pastor J, Kuro-o M, Liu X (2012) Nuclear localization of klotho in brain: An anti-aging protein. *Neurobiol Aging* 33:1483.e25–1483.e30.
11. Xu Y, Sun Z (2015) Molecular basis of klotho: From gene to function in aging. *Endocr Rev* 36:174–193.
12. Chen CD, et al. (2014) Identification of cleavage sites leading to the shed form of the anti-aging protein klotho. *Biochemistry* 53:5579–5587.
13. Imura A, et al. (2004) Secreted klotho protein in sera and CSF: Implication for post-translational cleavage in release of klotho protein from cell membrane. *FEBS Lett* 565:143–147.
14. Chen TH, et al. (2013) The secreted klotho protein restores phosphate retention and suppresses accelerated aging in klotho mutant mice. *Eur J Pharmacol* 698:67–73.
15. Nagai T, et al. (2003) Cognition impairment in the genetic model of aging *klotho* gene mutant mice: A role of oxidative stress. *FASEB J* 17:50–52.
16. Shiozaki M, et al. (2008) Morphological and biochemical signs of age-related neurodegenerative changes in klotho mutant mice. *Neuroscience* 152:924–941.
17. Li SA, et al. (2004) Immunohistochemical localization of klotho protein in brain, kidney, and reproductive organs of mice. *Cell Struct Funct* 29:91–99.
18. Clinton SM, et al. (2013) Expression of klotho mRNA and protein in rat brain parenchyma from early postnatal development into adulthood. *Brain Res* 1527:1–14.
19. Sathyanesan M, et al. (2012) A molecular characterization of the choroid plexus and stress-induced gene regulation. *Transl Psychiatry* 2:e139.
20. Semba RD, et al. (2014) Klotho in the cerebrospinal fluid of adults with and without Alzheimer's disease. *Neurosci Lett* 558:37–40.
21. Duce JA, et al. (2008) Gene profile analysis implicates klotho as an important contributor to aging changes in brain white matter of the rhesus monkey. *Glia* 56:106–117.
22. Liu F, Wu S, Ren H, Gu J (2011) Klotho suppresses RIG-I-mediated senescence-associated inflammation. *Nat Cell Biol* 13:254–262.
23. Massó A, et al. (2015) Secreted and transmembrane αKlotho isoforms have different spatio-temporal profiles in the brain during aging and Alzheimer's disease progression. *PLoS One* 10:e0143623.
24. Olauson H, et al. (2012) Targeted deletion of klotho in kidney distal tubule disrupts mineral metabolism. *J Am Soc Nephrol* 23:1641–1651.
25. Henry CJ, Huang Y, Wynne AM, Godbout JP (2009) Peripheral lipopolysaccharide (LPS) challenge promotes microglial hyperactivity in aged mice that is associated with exaggerated induction of both pro-inflammatory IL-1β and anti-inflammatory IL-10 cytokines. *Brain Behav Immun* 23:309–317.
26. Cribbs DH, et al. (2012) Extensive innate immune gene activation accompanies brain aging, increasing vulnerability to cognitive decline and neurodegeneration: A microarray study. *J Neuroinflammation* 9:179.
27. Baruch K, et al. (2013) CNS-specific immunity at the choroid plexus shifts toward destructive Th2 inflammation in brain aging. *Proc Natl Acad Sci USA* 110:2264–2269.
28. Mach B, Steimle V, Martinez-Soria E, Reith W (1996) Regulation of MHC class II genes: Lessons from a disease. *Annu Rev Immunol* 14:301–331.
29. Ebner F, et al. (2013) Microglial activation milieu controls regulatory T cell responses. *J Immunol* 191:5594–5602.

Zhu et al.

NEUROSCIENCE

30. Owens T, Khorooshi R, Wlodarczyk A, Asgari N (2014) Interferons in the central nervous system: A few instruments play many tunes. *Glia* 62:339–355.
31. Mesquita SD, et al. (2015) The choroid plexus transcriptome reveals changes in type I and II interferon responses in a mouse model of Alzheimer's disease. *Brain Behav Immun* 49:280–292.
32. Baruch K, et al. (2014) Aging. Aging-induced type I interferon response at the choroid plexus negatively affects brain function. *Science* 346:89–93.
33. Baruch K, Schwartz M (2013) CNS-specific T cells shape brain function via the choroid plexus. *Brain Behav Immun* 34:11–16.
34. Kunis G, et al. (2013) IFN-γ-dependent activation of the brain's choroid plexus for CNS immune surveillance and repair. *Brain* 136:3427–3440.
35. Goldmann T, et al. (2016) Origin, fate and dynamics of macrophages at central nervous system interfaces. *Nat Immunol* 17:797–805.
36. Leal SL, Yassa MA (2015) Neurocognitive aging and the hippocampus across species. *Trends Neurosci* 38:800–812.
37. Prinz M, Priller J (2014) Microglia and brain macrophages in the molecular age: From origin to neuropsychiatric disease. *Nat Rev Neurosci* 15:300–312.
38. Perry VH, Holmes C (2014) Microglial priming in neurodegenerative disease. *Nat Rev Neurol* 10:217–224.
39. Bennett ML, et al. (2016) New tools for studying microglia in the mouse and human CNS. *Proc Natl Acad Sci USA* 113:E1738–E1746.
40. Kurosu H, et al. (2006) Regulation of fibroblast growth factor-23 signaling by klotho. *J Biol Chem* 281:6120–6123.
41. Urakawa I, et al. (2006) Klotho converts canonical FGF receptor into a specific receptor for FGF23. *Nature* 444:770–774.
42. Yoshihara E, et al. (2014) Thioredoxin/Txnip: Redoxisome, as a redox switch for the pathogenesis of diseases. *Front Immunol* 4:514.
43. Zhou R, Tardivel A, Thorens B, Choi I, Tschopp J (2010) Thioredoxin-interacting protein links oxidative stress to inflammasome activation. *Nat Immunol* 11:136–140.
44. Oslowski CM, et al. (2012) Thioredoxin-interacting protein mediates ER stress-induced β cell death through initiation of the inflammasome. *Cell Metab* 16:265–273.
45. Spindel ON, World C, Berk BC (2012) Thioredoxin interacting protein: Redox dependent and independent regulatory mechanisms. *Antioxid Redox Signal* 16:587–596.
46. Bikle DD (2009) Extra renal synthesis of 1,25-dihydroxyvitamin D and its health implications. *Clin Rev Bone Miner Metab* 7:114–125.
47. Han N, Xu J, Xu F, Liu Z, Yin J (2016) The *in vivo* effects of a fraction from Dioscorea spongiosa on glucocorticoid-induced osteoporosis. *J Ethnopharmacol* 185:53–59.
48. Martinon F, Mayor A, Tschopp J (2009) The inflammasomes: Guardians of the body. *Annu Rev Immunol* 27:229–265.
49. Youm YH, et al. (2013) Canonical Nlrp3 inflammasome links systemic low-grade inflammation to functional decline in aging. *Cell Metab* 18:519–532.
50. Abderrazak A, et al. (2015) NLRP3 inflammasome: From a danger signal sensor to a regulatory node of oxidative stress and inflammatory diseases. *Redox Biol* 4:296–307.
51. Mariathasan S, et al. (2006) Cryopyrin activates the inflammasome in response to toxins and ATP. *Nature* 440:228–232.
52. Kuida K, et al. (1995) Altered cytokine export and apoptosis in mice deficient in interleukin-1 β converting enzyme. *Science* 267:2000–2003.
53. Kayagaki N, et al. (2011) Non-canonical inflammasome activation targets caspase-11. *Nature* 479:117–121.
54. Chen L, Eapen MS, Zosky GR (2017) Vitamin D both facilitates and attenuates the cellular response to lipopolysaccharide. *Sci Rep* 7:45172.
55. Simon MJ, Iliff JJ (2016) Regulation of cerebrospinal fluid (CSF) flow in neurodegenerative, neurovascular and neuroinflammatory disease. *Biochim Biophys Acta* 1862:442–451.
56. Samson RD, Barnes CA (2013) Impact of aging brain circuits on cognition. *Eur J Neurosci* 37:1903–1915.
57. Patterson SL (2015) Immune dysregulation and cognitive vulnerability in the aging brain: Interactions of microglia, IL-1β, BDNF and synaptic plasticity. *Neuropharmacology* 96:11–18.
58. Ning S, Pagano JS, Barber GN (2011) IRF7: Activation, regulation, modification and function. *Genes Immun* 12:399–414.
59. Perrone L, Devi TS, Hosoya K, Terasaki T, Singh LP (2009) Thioredoxin interacting protein (TXNIP) induces inflammation through chromatin modification in retinal capillary endothelial cells under diabetic conditions. *J Cell Physiol* 221:262–272.
60. Heneka MT, et al. (2013) NLRP3 is activated in Alzheimer's disease and contributes to pathology in APP/PS1 mice. *Nature* 493:674–678.
61. Dalton G, et al. (2017) Soluble klotho binds monosialoganglioside to regulate membrane microdomains and growth factor signaling. *Proc Natl Acad Sci USA* 114:752–757.
62. Maekawa Y, et al. (2009) Klotho suppresses TNF-α-induced expression of adhesion molecules in the endothelium and attenuates NF-kappaB activation. *Endocrine* 35:341–346.
63. Zhou X, Chen K, Lei H, Sun Z (2015) Klotho gene deficiency causes salt-sensitive hypertension via monocyte chemotactic protein-1/CC chemokine receptor 2-mediated inflammation. *J Am Soc Nephrol* 26:121–132.
64. Pothlichet J, et al. (2013) Type I IFN triggers RIG-I/TLR3/NLRP3-dependent inflammasome activation in influenza A virus infected cells. *PLoS Pathog* 9:e1003256.
65. Koo JW, Duman RS (2008) IL-1β is an essential mediator of the antineurogenic and anhedonic effects of stress. *Proc Natl Acad Sci USA* 105:751–756.
66. Stephan AH, et al. (2013) A dramatic increase of C1q protein in the CNS during normal aging. *J Neurosci* 33:13460–13474.
67. Heneka MT, et al. (2015) Neuroinflammation in Alzheimer's disease. *Lancet Neurol* 14:388–405.
68. Czirr E, Wyss-Coray T (2012) The immunology of neurodegeneration. *J Clin Invest* 122:1156–1163.
69. Schlögl M, Holick MF (2014) Vitamin D and neurocognitive function. *Clin Interv Aging* 9:559–568.
70. Cissé M, et al. (2011) Ablation of cellular prion protein does not ameliorate abnormal neural network activity or cognitive dysfunction in the J20 line of human amyloid precursor protein transgenic mice. *J Neurosci* 31:10427–10431.
71. Trouplin V, et al. (2013) Bone marrow-derived macrophage production. *J Vis Exp*, e50966.
72. Harris JA, et al. (2012) Human P301L-mutant tau expression in mouse entorhinal-hippocampal network causes tau aggregation and presynaptic pathology but no cognitive deficits. *PLoS One* 7:e45881.
73. Maeda S, et al. (2016) Expression of A152T human tau causes age-dependent neuronal dysfunction and loss in transgenic mice. *EMBO Rep* 17:530–551.
74. Stein LR, et al. (2014) Expression of Nampt in hippocampal and cortical excitatory neurons is critical for cognitive function. *J Neurosci* 34:5800–5815.
75. Livak KJ, Schmittgen TD (2001) Analysis of relative gene expression data using real-time quantitative PCR and the $2^{(-\Delta\Delta C(T))}$ method. *Methods* 25:402–408.